Adsorption of proteins on TiO2 particles influences their aggregation and cell penetration

Romain Vian, Hamideh Salehi, Marion Lapierre, Frédéric Cuisinier, Vincent Cavaillès, Sebastien Balme

Adsorption of proteins on TiO_2 particles influences their aggregation and cell penetration

Romain Vian[1$], Hamideh Salehi[2$], Marion Lapierre[1], Fréderic Cuisinier[2], Vincent Cavaillès[1§], Sébastien Balme[3§*]

[1]*IRCM, Institut de Recherche en Cancérologie de Montpellier, INSERM U1194, Université Montpellier, Montpellier F-34298, France*

[2]*LBN, Univ Montpellier, Montpellier, France*

[3]*IEM, Institut Européen des Membranes, UMR 5635 Université Montpellier, CNRS, ENSCM, Place Eugene Bataillon, F-34095 Montpellier cedex 5, France*

[$,§] *equal contribution*

[*] *corresponding author: tel: (33) 4 67 14 91 18; mail: Sebastien.balme@umontpellier.fr*

Abstract

TiO_2 nanoparticles known as E171 are one controversial food additive due to its potential toxicity. In this work, the main hypothesis is that the proteins adsorbed on the TiO_2 nanoparticles prevent their aggregation and favor the cell penetration. To do so, the TiO_2 nanoparticles were coated with gelatin and β-lactoglobulin (two proteins commonly found in food) to reach interfacial concentrations about 0.25 mg/mg and 0.32 mg/mg, respectively. The measurement of NP size showed that the protein coating improve the colloidal stability of TiO_2 nanoparticles. The FTIR analysis suggests that the β-lactoglobulin structure is modified after adsorption. Then, the penetration of TiO_2 penetration inside human intestinal epithelial cells was shown and quantify by using confocal Raman microscopy. Finally, the promoting role of the protein coating on the cell penetration was demonstrated for both the gelatin and β-lactoglobulin.

1. Introduction

Nanoparticles (NP) are commonly used in food as texturing and flavor agents (McCracken et al., 2016). One widely used additive is the food grade TiO_2 also identified as E171, which is found in various food products (including candies and chocolate bars) as well as toothpaste. In 2012, a simulation of $Ti0_2$ consumption emphasizes that children below 10 years old are the most exposed individuals (Weir et al., 2012). TiO_2 is also used for packaging and, in that case, food can be contaminated by the packing (Lin et al., 2014). The question about the innocuousness of TiO_2 nanoparticles (TiO_2 NP) is not new since in 2011, Skocaj et al. addressed the question: "Titanium dioxide in our everyday life; is it safe?" (Skocaj et al., 2011). Closer than 10 years after, the impact of food grade TiO_2 on health is not totally elucidated and there is a need for interdisciplinary approaches to understand organ/NP interaction (Chaudhry et al., 2008).

Numerous effects of TiO_2 have been reported on different organs such as liver, brain, intestines or spleen (Jovanović, 2015). The TiO_2 NPs are known as inducers of inflammation in several organs such as kidney (Gui et al., 2011). In addition, genotoxicity has been observed for numerous structures of TiO2 NPs (including anatase and rutile) with different exposure modes (ingestion, inhalation...) (Shi et al., 2013). The TiO_2 NPs induce oxidative damages to DNA. The E171 toxicity on intestinal cells is moderated but sufficient to suggest a role in tumor growth in the colon of mice (Dorier et al., 2017; Proquin et al., 2018). Moreover, E171 is suspected to worsen existing intestinal disease (Urrutia-Ortega et al., 2016). Indeed, the sedimentation of TiO_2 could induce a loss of intestinal microvilli (Faust et al., 2014) and a slight deregulation of the fatty acids profiles in the intestine. However, the TiO_2 NPs do not seem to impact the bacteria gas production (Dudefoi et al., 2017). Finally, in cells, TiO_2 NPs were found to disrupt the structure of lysosomes and to damage the mitochondria (Zhang et al., 2018) and could have synergy action with food molecules such as glucose (Wang et al., 2013).

49 The relevant properties which explain NP toxicity are their solubility, shape, surface charge, size
50 distribution and structure (McCracken et al., 2016). Cell penetration was reported after dermal
51 exposure and in hairless skin, TiO_2 NPs were found in epidermis cells (Wu et al., 2009). Basically,
52 TiO_2 NPs can penetrate in cells as shown for MCF-7 and TERT cells using confocal Raman
53 spectroscopy (Salehi et al., 2014). Recently, debate around the use of $Ti0_2$ in food was revived. In
54 2017, Bettini et *al*. reported that after 100 days, the TiO_2 nanoparticles initiate preneoplastic
55 lesions and promote colon inflammation. This suggested a potential role of TiO_2 NPs in
56 autoimmune disease and colorectal cancers (Bettini et al., 2017). Following this publication, the
57 French Agency for Food, Environmental and Occupational Health and Safety has recommended
58 the limitation the TiO_2 as food additive as emergency measure regarding the lack of knowledge
59 about the real toxicity (Anses, 2019).
60 As the other nanoparticles, TiO_2 tends to aggregate in solution. This is enhanced by the presence
61 of salt in the media (Allouni et al., 2009). The ability of proteins to prevent nanoparticle
62 aggregation is well known (Lepoitevin et al., 2015). For noble metals, such property is modulated
63 to design colorimetric sensors (Sabela et al., 2017). The coating of TiO_2 NPs by human serum
64 albumin, bovine serum albumin or fetal bovine serum prevents the aggregation process (Allouni
65 et al., 2009; Yusoff et al., 2018). In their review, McCracken et al. hypothesized that NP coating by
66 protein could be an important factor of their toxicity (McCracken et al., 2016).
67 Protein adsorption on material is a complex and fascinating phenomena whose mechanism is not
68 fully understood after several decades of investigation. However, the structural classification of
69 proteins could be a way to predict their behavior on a flat surface (Coglitore et al., 2019).
70 Numerous parameters affect protein adsorption on nanoparticles such as pH, concentration,
71 temperature, salt concentration (Bhakta et al., 2015) and additional molecules such as polyphenol
72 (Coglitore et al., 2018). Hard proteins such as lysozyme keep their structure after adsorption on

73 solid interface (Balme et al., 2013). Although considered as soft protein, BSA does not unfold on
74 food grade E171 (Kim & Doudrick, 2019). The adsorption of blood proteins on anatase TiO_2 NPs
75 affects the agglomerate size and surface charge. Additionally, this altered the electrostatic binding
76 affinity with fibroblasts (Allouni et al., 2015). Because proteins can strongly interact with TiO_2 NPs,
77 we addressed the question about the consequences of such interaction. Typically, under salted
78 media, NP aggregation reduces the ability of the NP to penetrate inside the cell. Food proteins,
79 by preventing this aggregation process, could therefore enhance the penetration of TiO_2 NPs in
80 the cell. In order to verify this hypothesis, we selected two proteins *i.e.* β-lactoglobulin and gelatin.
81 β-lactoglobulin is mainly composed of β-sheets which provide a high internal energy. In presence
82 of silica or hydrophobic surface, the conformational changes of β-lactoglobulin are small
83 (Wahlgren & Arnebrant, 1990). When β-lactoglobulin is adsorbed on clay, only weak structural
84 modification occur (Assifaoui et al., 2014). The second protein is gelatin, which is widely used in
85 candies mixed with E171. Gelatin interacts with TiO_2 NPs and such interaction has been used to
86 pattern TiO2 porous microspheres (Liu et al., 2015). However, the main application of gelatin TiO2
87 composite is food packaging (He et al., 2016).
88 Mostly, intracellular imaging methods, such as electron microscopy, cryoelectron microscopy, and
89 immunofluorescence microscopy, due to the fixation, freezing and use of dyes or biomarkers are
90 destructive and harmful to the cells. As Raman spectroscopy does not need chemical fixation,
91 markers, or genetic modifications, it is considered as a non-invasive imaging method (Klein et al.,
92 2012; Salehi et al., 2013). Raman spectroscopy is based on inelastic scattering of photons from
93 the incident wavelength. The monochromatic light interacting with the sample, produces a
94 Raman spectrum, composing different bands related to the vibrational frequencies of different
95 functional groups. Subsequently every molecule has an exclusive fingerprint or Raman spectrum.
96 The high spatial resolution and possibility of imaging in aqueous environment make Raman

97 microscopy an ideal tool for life and fixed imaging of a single cell (Salehi et al., 2014). The adequate
98 data analysis according to the vibrational spectra of different cellular organelles, anticancer drugs
99 or nanoparticles provides alternative to existing methods for cell imaging under normal
100 physiological conditions (Gulka et al., 2020; Salehi et al., 2018). The unique spectral signature of
101 nanoparticles enable tracing coated/ non-coated TiO_2 cellular penetration.
102 As previously mentioned, the toxicity of TiO_2 was demonstrated on different type cells in vitro as
103 well as in-vivo. In these cases, numerous external parameters can influence the cell penetration
104 of the nanoparticle including the protein adsorption. This work aims to verify for the first time the
105 hypothesis of the role the protein coating on the TiO_2 nanoparticle cell penetration. Indeed, this
106 question is motivated to elucidate the first step mechanism of the tiO_2 toxicity. To do so, gelatin
107 and β-lactoglobulin adsorption on TiO_2 rutile was first investigated to determine their surface
108 concentration and eventual structural modifications. Then, we evaluated the impact of each of
109 the two proteins on TiO_2 NPs aggregation. Finally, the penetration of NPs coated or not with
110 proteins was investigated by confocal Raman microscopy.
111
112 **2. Materials and methods**
113 **a. Preparation of NPs**
114 The titanium dioxide (TiO_2) powder (99% rutile) (SIGMA) was suspended in distilled water at a
115 concentration of 1 mg/ml. The solution was then sonicated for 1 hour at 60°C (ref sonicator: ELMA
116 Ultrasonic Cleaner S100H) to break up any interactions that may have formed between the
117 different particles. Gelatin (L3908) and β-lactoglobulin (G6144) from Sigma were dissolved in
118 distilled water at a concentration of 1 mg/ml and sonicated. Three solutions were prepared at a
119 final concentration of 0.75 mg/ml of TiO_2 NPs: NPs alone, NPs with gelatin and NPs with β-
120 lactoglobulin. In these solutions, the ratio was about 3 TiO_2 NPs to 1 protein. In order to promote

121 the adsorption of these proteins on NPs as effectively as possible, the solutions were placed on
122 an agitator for one hour at room temperature and then stored at 4°C. A sonication of 5 minutes
123 at room temperature for coated rated NPs and one hour at 60°C for unrated uncoated NPs was
124 applied before each use.

125 ***b.*** **Characterization of protein adsorption**

126 The interfacial concentration of protein on TiO_2 NPs was obtained by the method of supernatant
127 depletion previously reported (Lepoitevin et al., 2014). Briefly, after incubation, the mixtures
128 containing TiO_2 NPs and proteins were centrifuged (15 min at 15000 rpm). Protein concentration
129 in the supernatant was determined by UV-Vis absorption (Jasco) at 290 nm. The structural
130 modifications of adsorbed protein were characterized by ATR-FTIR (Nexus) under D_2O. The
131 measurement of NP size was performed by Dynamic Light Scattering (DLS) (Nanophox) using a
132 laser light of 632 nm. For each condition or type of NPs, the measurement was carried out in
133 triplicate. Several parameters such as medium (water, DMEM/F12 medium and RPMI medium)
134 condition and time (from day 0 to day 5) were modified between different measurements. The
135 data analysis was done using QuickFit software.

136 **c. Cell culture**

137 HT29 human colon adenocarcinoma cells were grown in DMEM/F12 medium (M1) or RPMI
138 medium (M2) supplemented with 10% FCS, 100U/ml penicillin, 100 mg/ml streptomycin and
139 100 mg/ml sodium pyruvate. For Raman experiments, $3x10^5$ HT-29 cells were cultivated for 24 h
140 onto polished and disinfected calcium fluoride CaF_2 (Crystran Ltd, Dorset, UK) substrates in 35 mm
141 Petri dishes. After cell adherence to the substrate, the cells were incubated with dissolved
142 nanoparticle solutions at 2 µg/mL concentration for one hour. The cells on the CaF_2 substrates
143 were then fixed with 2% PFA (paraformaldehyde) after thorough rinsing with PBS. Cells were kept
144 in PBS and transferred directly for Raman measurements. Before carrying out measurements of

TiO_2 on the cells, several reference spectra of the different NP solutions were carried out for 4 conditions, TiO_2 powder and the three solutions of TiO_2 coated or not by proteins (NP/NPG/NPL).

d. Analysis of cell penetration by Raman microscopy

Raman data acquisition

To collect the Raman spectra, Witec Confocal Raman Microscope System alpha 300R (Witec Inc., Ulm, Germany) was used. The excitation light in confocal Raman microscopy was generated via a frequency-doubled Nd:YAG lasers (New-port, Irvine, CA, USA) at a wavelength of 532 nm. A 60× NIKON water immersion objective with a numerical aperture of 1.0 and a working distance of 2.8 mm (Nikon, Tokyo, Japan) was used to focus the laser beam onto the cells. The laser power after the objective was 15 mW but finally, lower power was absorbed by cells in PBS. The scattered radiation goes through an edge filter to the electron multiplying charge coupled device camera EMCCD (DU 970N-BV353, Andor, Hartford, USA). The EMCCD chip size was 1600 × 200 pixels, the camera controller of a 16-bit A/D converter operated at 2.5 MHz. The acquisition time of a single spectrum was set to 0.5 sec. A zone of 150 × 150 pixels (spatial unit) per image was recorded, giving 22500 spectra for one image. Data acquisition and analysis was performed using Image Plus 2.08 Witec software. A spatial resolution of 300 nm and a depth resolution of 1µm were measured for the system. Considering the limit of Raman microscope (300 nm), the measurements of particle sizes on each image (processed and analyzed using Witec software) were done by zooming on particles and using line size measurement tool.

Raman data analysis

Two data analysis methods have been applied. The first method presented integrated Raman intensities in specific regions in particular C-H stretching mode. The lipid-protein distribution in the cells is shown by the integrated Raman intensities of C-H stretching mode (2800–3000cm^{-1}) using Image Plus software, Witec. Consequently, a map of the region regarding these integrated

intensities was provided. A false color image of CH Raman peak contains bright yellow hues for the highest intensities and dark orange hues for the lowest integrated intensities. K-mean cluster analysis (KMCA) as the second data analysis method separated data into k-mutually clusters. KMCA was done using the Witec Project Plus (Ulm, Germany) software.

e. Statistical analysis

All experiments were conducted independently at least three times. Results were expressed as the mean ± standard error of the mean (S.E.M). Statistical comparisons were performed with one-way ANOVA or t-test as indicated. A probability level (p value) of 0.05 was chosen for statistical significance.

3. Results and discussion

a. Protein adsorption on TiO_2 NPs

Prior to the investigation of the protein impact on colloidal stability and cell penetration, we characterized protein loading on TiO_2 NPs. Indeed, the protein/NP interaction is extremely dependent on the intrinsic properties of the material and on the media. Here, we have used water in order to prevent salt induced aggregation of TiO_2 NPs and thus to optimize the accessible surface of NPs for protein adsorption.

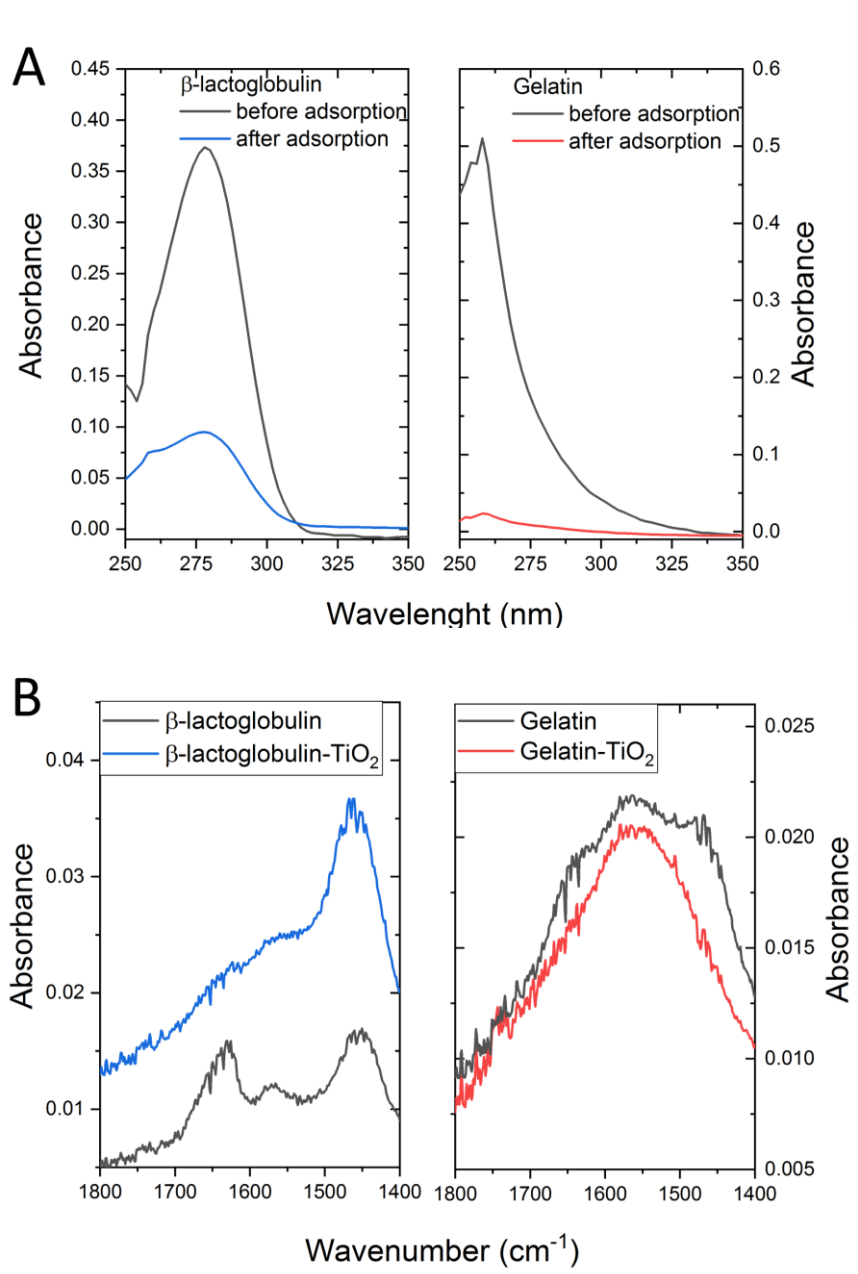

Figure 1: (A) Absorbance spectra of β-lactoglobulin (left) and gelatin (right) before (black line) and after (red line) contact with TiO_2 NPs at a concentration of 0.75 mg/ml for 1 hour. (B) FTIR spectra of β-lactoglobulin (left) and gelatin (right) in D_2O (black line) and loaded on TiO_2 NPs (blue or red line)

The interfacial concentration of protein was determined from the depletion of supernatant method. Figure 1A shows the absorbance spectra for β-lactoglobulin and gelatin before and after

adsorption on TiO_2 NPs. We can observe a large decrease of protein concentration in solution upon adsorption. The interfacial concentrations for β-lactoglobulin and gelatin were found about 0.25 mg/mg and 0.32 mg/mg of TiO_2 NPs, respectively.

We attempted to obtain information about the structural modifications of proteins induced by their adsorption on TiO_2 NPs. In Figure 1B are plotted the FTIR spectra recorded under D_2O. For the β-lactoglobulin, the band in 1640 cm^{-1} was assigned to the amide I. In D_2O, the amides II gave two bands in 1560 cm^{-1} and 1455 cm^{-1} relative to N-H and N-D bonds, respectively. This emphasizes the accessibility to the solvent of the amide II moieties to exchange H by D. After loading on TiO_2 NPs, the 3 bands were still present. Unfortunately, the absorption of Ti-OD bond about 1590 made a deep structural analysis impossible. However, we observed an increase of the band in 1455 cm^{-1} that could be assigned to the conversion of N-H to N-D. This suggested that the amides I bound with H were more exposed to the solvent after loading on TiO_2 NPs due to structural modifications.

For gelatin in D_2O, the 3 bands were also present but more difficult to distinguish because of the low order degree of the protein. However, we noticed that the two bands of amides I were large showing the existence of N-H and N-D bonds. After loading, the band about 1690 cm^{-1} masked the other ones. Conversely to β-lactoglobulin, the adsorption of gelatin did not seem to promote the exposition of the amides II to the solution.

b. Colloidal stability of TiO_2 NPs with and without protein loading

As previously mentioned, the colloidal stability of TiO_2 NPs could strongly be affected by protein adsorption. Importantly, this is also a key factor for cell penetration. Thus, we then investigated by dynamic light scattering the TiO_2 NP size, in water and in two cell culture media.

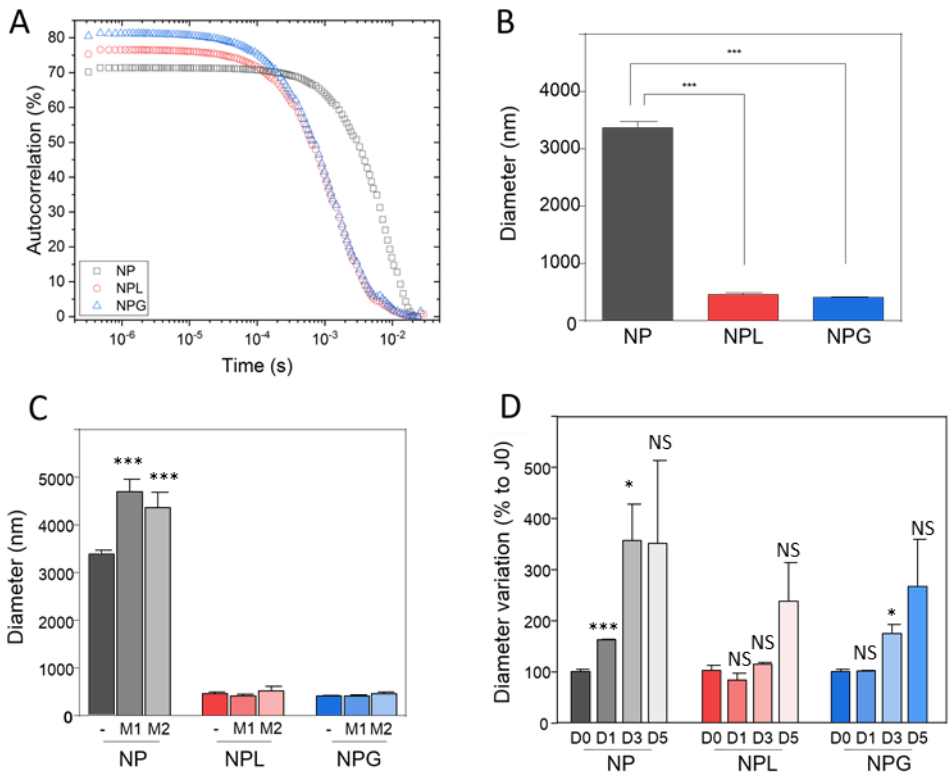

Figure 2: Nanoparticle size by diffusion light scattering (A) Autocorrelation function of TiO_2 NPs without (black) and with protein (in red, β-lactoglobulin and in blue, gelatin). The sizes of TiO_2 NPs are obtained in water (B) and culture media (DMEM/F12 medium (M1) or RPMI medium (M2)) (C). (D) Size evolution of the small component as a function of time (From Day 0 to Day 5). TiO_2 NPs alone is noted NP, TiO_2 NPs with gelatin is noted NPG and TiO_2-NPs with β-lactoglobulin is noted NPL. Statistical significance is shown as p-value from one-way Anova test (panels B and C) or t-test in panel D (*: $p < 0.05$; ***: $p < 0.001$).

In Figure 2A, the autocorrelation functions for TiO_2 NPs in water, with and without proteins are reported. We observed a shift toward short times when TiO_2 NPs were coated with proteins. At first approximation, the autocorrelation functions were fitted with only one component to obtain an average size distribution. For uncoated TiO_2 NPs, the distribution was centered around 3.2 µm

228 while after protein coating it was about 400 nm (Figure 2B). This is due to a rapid aggregation of
229 TiO_2 NPs after sonication. Here, we can note that both gelatin and β-lactoglobulin prevented the
230 fast aggregation phenomena of TiO_2 NPs.
231 In general, NP aggregation is favored by salt addition. Thus, similar analyses were performed using
232 two different media used for cell culture (Figure 2C). This experiment was also motivated because
233 the role of protein loading cannot be predicted since it is dependent on the protein and the
234 eventual binding with small molecules, as shown for gold NP (Coglitore et al., 2018; Lepoitevin et
235 al., 2015) or clay mineral (Trigueiro et al., 2018).
236 As expected, the size of raw TiO_2 NPs increased due to salt-induced aggregation. Conversely,
237 coating with proteins appeared to prevent the aggregation process. These results agree with
238 previous investigations showing that the extracellular polymeric substances from *Bacillus subtilis*
239 improve the colloidal stability of TiO_2 NPs (Di Lin et al., 2017; Di Lin et al., 2016). Gelatin has a low
240 internal energy structure and thus can optimize its conformation around the TiO_2 NPs. Conversely,
241 β-lactoglobulin is mainly composed of β-sheet, has a high internal energy and is positively charged
242 at pH 7.4. However, the FTIR revealed structural modifications, which probably allowed the
243 interaction between the protein and TiO_2 NPs. This means that the electrostatic interaction
244 between the TiO_2 NPs and β-lactoglobulin are not shielded by salt addition thus explaining the
245 colloidal stability.
246 TiO_2 NPs penetrate inside cells only if their size are hundreds nanometer scale. The low accuracy
247 of the autocorrelation fit with only one component suggested a polydispersity of the samples. To
248 further analysis the size of TiO_2 NPs, we separated two populations from the autocorrelation
249 curves. A first population with a diameter below 100 nm was assigned to non-aggregated
250 particles. The second population micrometer scale corresponded to aggregates. The relative
251 weight of each population showed that non-aggregated particles were the main one (upper than

252 99%), for the TiO_2 NPs coated with proteins. We then focused on this population more prone to
253 penetrate inside the cells. The stability of these small TiO_2 NPs as a function of time was
254 investigated for duration up to 5 days (Figure 2D). Without protein coating, TiO_2 NPs were prone
255 to aggregate with time as monitored by the diameter variation as a function of the time. Typically,
256 at D0 the mean size of the TiO_2-NP was about 100 nm and reached 480 nm after D5. This is not
257 surprising since TiO_2 NPs are not stable in solution. With gelatin, the TiO_2 NPs size was stable until
258 D1 around 91 nm. Then, the diameter variation increased to reach 250 % at D5. Finally, β-
259 lactoglobulin offered the most effective protection against aggregation since the size of NPL
260 particles remained constant during the 3-days.
261 At this stage, we demonstrated that protein coating prevented the TiO_2 NPs aggregation in water
262 as well as in salt media. On the other hand, the colloidal stability was also improved during the
263 time especially for the β-lactoglobulin.

264 **c. Effect of proteins on cell penetration of TiO_2 NPs**

265 To find out the role of protein, intracellular penetration of TiO_2 NPs was investigated using the
266 human intestinal epithelial cell lines HT-29, cultured in DMEM-F12 medium. The characterization
267 of TiO_2 NPs and their location were obtained using confocal Raman microscopy.
268 The Raman spectrum of TiO_2 powder showed three significant peaks at 275 cm^{-1}, 450 cm^{-1} and
269 610 cm^{-1} (Figure 3A). Coated/non-coated TiO_2 NPs in solution, showed the same peak position
270 confirming the integrity of TiO_2 NPs. The low intensities of TiO_2 NPs coated with proteins (blue and
271 red line for NPG and NPL, respectively) peaks were due to the coating, which avoids particles
272 accumulation and lower Raman signal. In addition, powder signal was higher as compared to the
273 NP in solution, as the number of particles under the laser spot was lower for the floating particles
274 in solution.
275

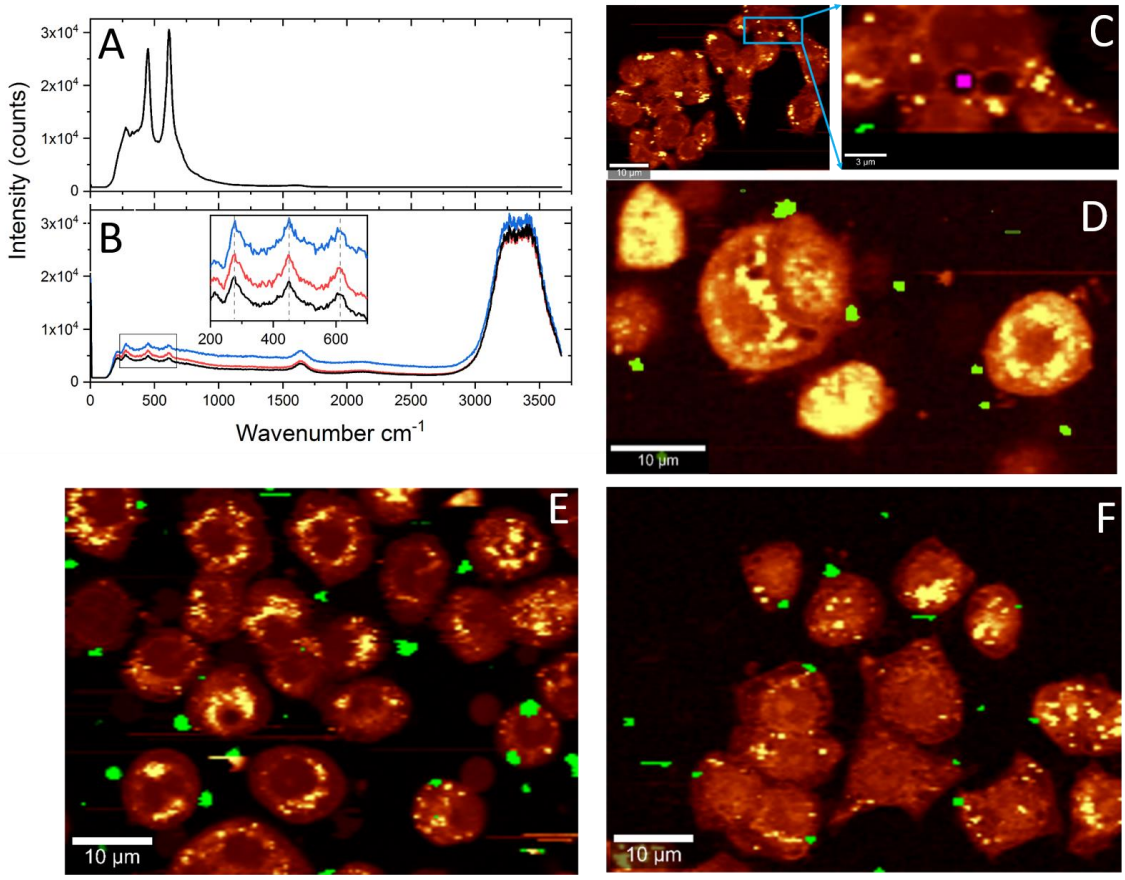

Figure 3: Raman spectra of (A) TiO_2 powder, (B) TiO_2-NPs (black line), TiO_2-NPs with gelatin (blue line) and TiO_2-NPs with β-lactoglobulin (red line), the inset is a zoom of 200 cm^{-1} – 700 cm^{-1} region. (C) Integration over Raman intensities of CH region, HT-29 cells incubated with TiO_2 NPGs and selected areas to focus on the TiO_2 presence inside the cell in pink color and outside in green. The image (D), (E) and (F) were obtained in presence of TiO_2-NPs, TiO_2-NPs with gelatin and TiO_2-NPs with β-lactoglobulin respectively.

Figure 3(B-E) illustrates the image acquisition of cells in presence of TiO_2 NPs with and without protein coating. Raman images present the biomolecules and two clusters in pink (intracellular penetrated particles) and green (extracellular particles). The intensity of CH bonds is plotted in yellow hues have the maximum intensity (for proteins or lipids) and dark hues have zero intensity

288 of CH bonds (background and out of cells). After 1 hour incubation of HT-29 cells with raw
289 nanoparticles, TiO_2 NPs aggregates were mainly present outside the cell or were in interaction
290 with the cell membrane. Conversely, TiO_2 NPs coated with proteins were found inside the cells
291 suggesting that protein coating favored cell penetration. We also noticed that TiO_2 NPs coated
292 with proteins were more abundant as compared to the particles without coating.
293 Further analysis reported on Figure 4 shows the percentage of total penetration of
294 coated/noncoated NPs. The quantification was obtained from a total number of 296 cells from all
295 the Raman images that were analyzed. The average size of TiO_2 NPs inside the cells showed that
296 the raw TiO_2 NPs were larger (1.4 µm) than the coated TiO_2 NPs (1 µm and 0.8 µm for gelatin and
297 β-lactoglobulin, respectively). The spatial resolution of Raman microscopy is 300 nm and thus a
298 discrepancy between the DLS is not surprising. Indeed, the Raman microscopy provides
299 information on several nanoparticles that can count one by one as soon as their size is larger than
300 the resolution while the DLS provides a means measurement of the nanoparticle size that can be
301 distorted in the case of heterogeneous samples. However, the tendency between confocal Raman
302 microscopy results and DLS measurements were in good agreement.
303 We also quantified the percentage of NPs that penetrated inside the cells (Figure 4B and C). For
304 the raw TiO_2 NPs, 35% of particles were located inside HT-29 cells. This ratio increased up to 42%
305 and 55% when the TiO2 NPs were coated with gelatin or β-lactoglobulin, respectively. Such
306 enhancement of cell penetration induced by protein coating was significant and probably linked,
307 at least in part, to the difference in size of the three types of NPs. We also evaluated the
308 distribution of TiO_2 NPs in the cell population. Without proteins, the TiO_2 NPs penetrated only 28%
309 of the cells. The coating with protein favored the dissemination of TiO_2 NPs since 48% and 70% of
310 cells showed internalized TiO_2 NPs after coating with gelatin and β-lactoglobulin, respectively. The

311 difference between the two proteins can be assigned to their ability to prevent the TiO_2 NPs
312 aggregation.
313 As demonstrated, confocal Raman microscopy with high spatial resolution allowed us to analyze
314 and trace coated/non-coated TiO2 nanoparticles. This label-free method using the spectral
315 fingerprint of nanoparticles permitted the monitoring of their intracellular penetration. The
316 results obviously present the significant difference between coated particles agglomeration and
317 penetration. Non-coated TiO_2 are more prone to aggregation and therefore their intracellular
318 penetration was lower. Conversely, protein adsorption prevented the TiO_2 NPs aggregation and
319 thus favored cell penetration.
320

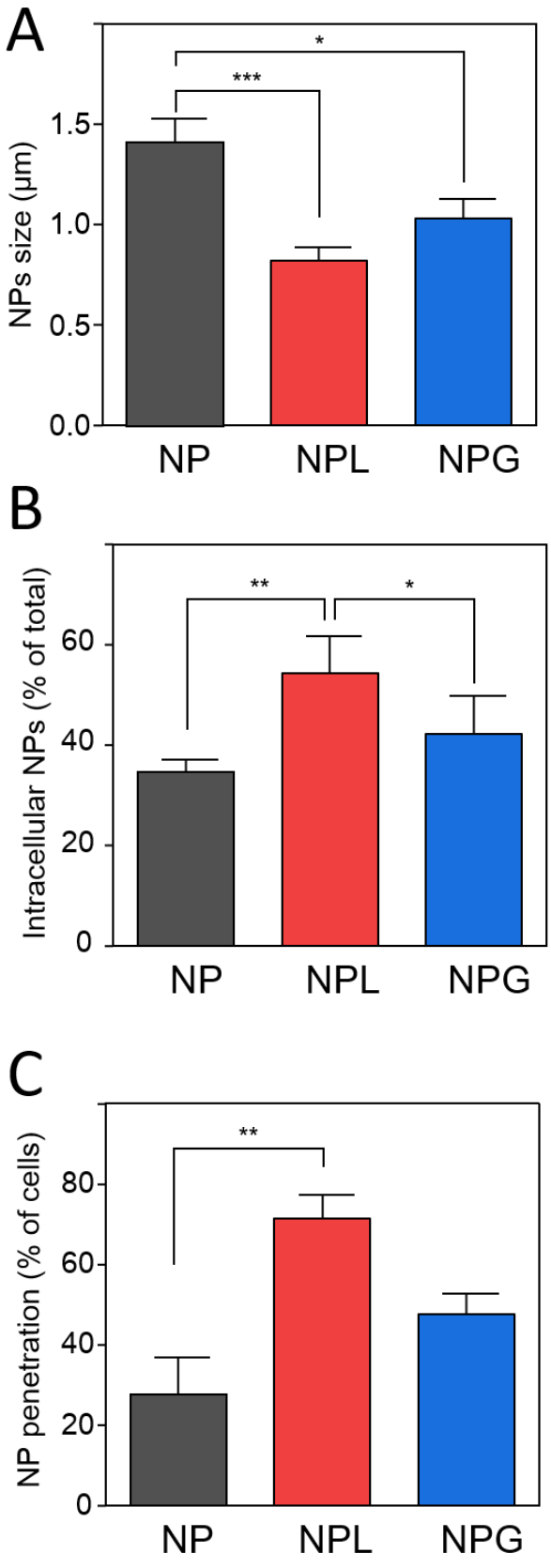
A
*
***
NPs size (μm)
1.5
1.0
0.5
0.0
NP
NPL
NPG
B
**
*
Intracellular NPs (% of total)
60
40
20
0
NP
NPL
NPG
C
**
NP penetration (% of cells)
80
60
40
20
0
NP
NPL
NPG

321

Figure 4: Characterization of TiO_2 NP penetration inside HT-29 cells (A) NP size, (B) ratio of intracellular TiO_2 NPs and (C) percentage of cells containing TiO_2 NPs. TiO_2 NPs alone is noted NP, TiO_2 NPs with gelatin is noted NPG, and TiO_2 NPs with β-lactoglobulin is noted NPL. Statistical significance is shown as p-value from one-way Anova test (*: $p<0.05$; **: $p<0.01$;*: $p<0.001$).**

4. Conclusion

To sum up, we investigated the impact of protein adsorption on cell penetration of TiO_2 NPs. Our results showed that both β-lactoglobulin and gelatin were loaded on TiO_2 NPs. The FTIR suggested that β-lactoglobulin (but not gelatin) adsorption induced a structural modification. The salt-induced aggregation and the colloidal stability were improved by protein adsorption. The cell penetration investigated by confocal Raman microscopy revealed that the β-lactoglobulin favored more efficiently than gelatin TiO_2 NP cell penetration. Moreover, our results showed a correlation between the ability of proteins to prevent NP aggregation and to facilitate cell penetration.

Overall, this work proves that proteins present in food have a significant impact on TiO_2 NP penetration in human intestinal epithelial cells. This tends to reinforce the hypothesis that NP coating by proteins could be an important factor explaining their toxicity. Thus, in further investigations aiming to understand the toxicity of TiO_2 NP, the role of food proteins should be taken into account.

Acknowledgments

This work was supported by the INCa-Cancéropole GSO (grant 2018-E02). Raman microscopy analysis during this study was realized using the EDMOS platform which was created with the

financial support of the Region Occitanie (France) and the European Regional Development Fund (ERDF).

References

Allouni, Z. E., Cimpan, M. R., Høl, P. J., Skodvin, T., & Gjerdet, N. R. (2009). Agglomeration and sedimentation of TiO2 nanoparticles in cell culture medium. *Colloids and surfaces. B, Biointerfaces*, *68*, 83–87.

Allouni, Z. E., Gjerdet, N. R., Cimpan, M. R., & Høl, P. J. (2015). The effect of blood protein adsorption on cellular uptake of anatase TiO2 nanoparticles. *International journal of nanomedicine*, *10*, 687–695.

Anses (2019). ANSES OPINION on the risks associated with ingestion of the food additive E171.

Assifaoui, A., Huault, L., Maissiat, C., Roullier-Gall, C., Jeandet, P., Hirschinger, J., Raya, J., Jaber, M., Lambert, J.-F., Cayot, P., Gougeon, R. D., & Loupiac, C. (2014). Structural studies of adsorbed protein (betalactoglobulin) on natural clay (montmorillonite). *RSC Adv*, *4*, 61096–61103.

Balme, S., Guégan, R., Janot, J.-M., Jaber, M., Lepoitevin, M., Dejardin, P., Bourrat, X., & Motelica-Heino, M. (2013). Structure, orientation and stability of lysozyme confined in layered materials. *Soft Matter*, *9*, 3188.

Bettini, S., Boutet-Robinet, E., Cartier, C., Coméra, C., Gaultier, E., Dupuy, J., Naud, N., Taché, S., Grysan, P., Reguer, S., Thieriet, N., Réfrégiers, M., Thiaudière, D., Cravedi, J.-P., Carrière, M., Audinot, J.-N., Pierre, F. H., Guzylack-Piriou, L., & Houdeau, E. (2017). Food-grade TiO2 impairs intestinal and systemic immune homeostasis, initiates preneoplastic lesions and promotes aberrant crypt development in the rat colon. *Scientific reports*, *7*, 40373.

Bhakta, S. A., Evans, E., Benavidez, T. E., & Garcia, C. D. (2015). Protein adsorption onto nanomaterials for the development of biosensors and analytical devices: a review. *Analytica chimica acta*, *872*, 7–25.

Chaudhry, Q., Scotter, M., Blackburn, J., Ross, B., Boxall, A., Castle, L., Aitken, R., & Watkins, R. (2008). Applications and implications of nanotechnologies for the food sector. *Food additives & contaminants. Part A, Chemistry, analysis, control, exposure & risk assessment*, *25*, 241–258.

Coglitore, D., Giamblanco, N., Kizalaité, A., Coulon, P. E., Charlot, B., Janot, J.-M., & Balme, S. (2018). Unexpected Hard Protein Behavior of BSA on Gold Nanoparticle Caused by Resveratrol. *Langmuir the ACS journal of surfaces and colloids*, *34*, 8866–8874.

Coglitore, D., Janot, J.-M., & Balme, S. (2019). Protein at liquid solid interfaces: Toward a new paradigm to change the approach to design hybrid protein/solid-state materials. *Advances in colloid and interface science*, *270*, 278–292.

Di Lin, Drew Story, S., Walker, S. L., Huang, Q., & Cai, P. (2016). Influence of extracellular polymeric substances on the aggregation kinetics of TiO2 nanoparticles. *Water research*, *104*, 381–388.

Di Lin, Story, S. D., Walker, S. L., Huang, Q., Liang, W., & Cai, P. (2017). Role of pH and ionic strength in the aggregation of TiO2 nanoparticles in the presence of extracellular polymeric substances from Bacillus subtilis. *Environmental pollution (Barking, Essex 1987)*, *228*, 35–42.

Dorier, M., Béal, D., Marie-Desvergne, C., Dubosson, M., Barreau, F., Houdeau, E., Herlin-Boime, N., & Carriere, M. (2017). Continuous in vitro exposure of intestinal epithelial cells to E171 food additive causes oxidative stress, inducing oxidation of DNA bases but no endoplasmic reticulum stress. *Nanotoxicology*, 1–11.

Dudefoi, W., Moniz, K., Allen-Vercoe, E., Ropers, M.-H., & Walker, V. K. (2017). Impact of food grade and nano-TiO2 particles on a human intestinal community. *Food and chemical toxicology an international journal published for the British Industrial Biological Research Association*, *106*, 242–249.

Faust, J. J., Doudrick, K., Yang, Y., Westerhoff, P., & Capco, D. G. (2014). Food grade titanium dioxide disrupts intestinal brush border microvilli in vitro independent of sedimentation. *Cell biology and toxicology*, *30*, 169–188.

Gui, S., Zhang, Z., Zheng, L., Cui, Y., Liu, X., Li, N., Sang, X., Sun, Q., Gao, G., Cheng, Z., Cheng, J., Wang, L., Tang, M., & Hong, F. (2011). Molecular mechanism of kidney injury of mice caused by exposure to titanium dioxide nanoparticles. *Journal of hazardous materials*, *195*, 365–370.

Gulka, M., Salehi, H., Varga, B., Middendorp, E., Pall, O., Raabova, H., Cloitre, T., Cuisinier, F. J. G., Cigler, P., Nesladek, M., & Gergely, C. (2020). Simultaneous label-free live imaging of cell nucleus and luminescent nanodiamonds. *Scientific reports*, *10*, 9791.

He, Q., Zhang, Y., Cai, X., & Wang, S. (2016). Fabrication of gelatin-TiO2 nanocomposite film and its structural, antibacterial and physical properties. *International journal of biological macromolecules*, *84*, 153–160.

Jovanović, B. (2015). Critical review of public health regulations of titanium dioxide, a human food additive. *Integrated environmental assessment and management*, *11*, 10–20.

Kim, J., & Doudrick, K. (2019). Emerging investigator series: protein adsorption and transformation on catalytic and food-grade TiO 2 nanoparticles in the presence of dissolved organic carbon. *Environmental Science: Nano*, *6*, 1688–1703.

Klein, K., Gigler, A. M., Aschenbrenner, T., Monetti, R., Bunk, W., Jamitzky, F., Morfill, G., Stark, R. W., & Schlegel, J. (2012). Label-free live-cell imaging with confocal Raman microscopy. *Biophysical journal*, *102*, 360–368.

Lepoitevin, M., Jaber, M., Guégan, R., Janot, J.-M., Dejardin, P., Henn, F., & Balme, S. (2014). BSA and lysozyme adsorption on homoionic montmorillonite: Influence of the interlayer cation. *Applied Clay Science*, *95*, 396–402.

Lepoitevin, M., Lemouel, M., Bechelany, M., Janot, J.-M., & Balme, S. (2015). Gold nanoparticles for the bare-eye based and spectrophotometric detection of proteins, polynucleotides and DNA. *Microchimica Acta*, *182*, 1223–1229.

Lin, Q.-B., Li, H., Zhong, H.-N., Zhao, Q., Xiao, D.-H., & Wang, Z.-W. (2014). Migration of Ti from nano-TiO_2-polyethylene composite packaging into food simulants. *Food additives & contaminants. Part A, Chemistry, analysis, control, exposure & risk assessment*, *31*, 1284–1290.

Liu, B., Xiao, J., Xu, L., Yao, Y., Costa, B. F.O., Domingos, V. F., Ribeiro, E. S., Shi, F.-N., Zhou, K., Su, J., Wu, H., Zhong, K., Paixão, J. A., & Gil, J. M. (2015). Gelatin-assisted sol–gel derived TiO2 microspheres for hydrogen storage. *International Journal of Hydrogen Energy*, *40*, 4945–4950.

McCracken, C., Dutta, P. K., & Waldman, W. J. (2016). Critical assessment of toxicological effects of ingested nanoparticles. *Environmental Science: Nano*, *3*, 256–282.

Proquin, H., Jetten, M. J., Jonkhout, M. C. M., Garduño-Balderas, L. G., Briedé, J. J., Kok, T. M. de, Chirino, Y. I., & van Loveren, H. (2018). Gene expression profiling in colon of mice exposed to food additive titanium dioxide (E171). *Food and chemical toxicology an international journal published for the British Industrial Biological Research Association*, *111*, 153–165.

Sabela, M., Balme, S., Bechelany, M., Janot, J.-M., & Bisetty, K. (2017). A Review of Gold and Silver Nanoparticle-Based Colorimetric Sensing Assays. *Advanced Engineering Materials*, *19*, 1700270.

Salehi, H., Al-Arag, S., Middendorp, E., Gergely, C., Cuisinier, F., & Orti, V. (2018). Dental pulp stem cells used to deliver the anticancer drug paclitaxel. *Stem cell research & therapy*, *9*, 103.

Salehi, H., Calas-Bennasar, I., Durand, J.-C., Middendorp, E., Valcarcel, J., Larroque, C., Nagy, K., Turzó K, K., Dekany, I., & Cuisinier, F. J. G. (2014). Confocal Raman spectroscopy to monitor intracellular penetration of TiO 2 nanoparticles. *Journal of Raman Spectroscopy*, *45*, 807–813.

Salehi, H., Derely, L., Vegh, A.-G., Durand, J.-C., Gergely, C., Larroque, C., Fauroux, M.-A., & Cuisinier, F. J. G. (2013). Label-free detection of anticancer drug paclitaxel in living cells by confocal Raman microscopy. *Applied Physics Letters*, *102*, 113701.

Shi, H., Magaye, R., Castranova, V., & Zhao, J. (2013). Titanium dioxide nanoparticles: a review of current toxicological data. *Particle and fibre toxicology*, *10*, 15.

Skocaj, M., Filipic, M., Petkovic, J., & Novak, S. (2011). Titanium dioxide in our everyday life; is it safe? *Radiology and oncology*, *45*, 227–247.

Trigueiro, P., Pedetti, S., Rigaud, B., Balme, S., Janot, J.-M., Dos Santos, I. M. G., Gougeon, R., Fonseca, M. G., Georgelin, T., & Jaber, M. (2018). Going through the wine fining: Intimate dialogue between organics and clays. *Colloids and surfaces. B, Biointerfaces*, *166*, 79–88.

Urrutia-Ortega, I. M., Garduño-Balderas, L. G., Delgado-Buenrostro, N. L., Freyre-Fonseca, V., Flores-Flores, J. O., González-Robles, A., Pedraza-Chaverri, J., Hernández-Pando, R., Rodríguez-Sosa, M., León-Cabrera, S., Terrazas, L. I., van Loveren, H., & Chirino, Y. I. (2016). Food-grade titanium dioxide exposure exacerbates tumor formation in colitis associated cancer model. *Food and chemical toxicology an international journal published for the British Industrial Biological Research Association*, *93*, 20–31.

Wahlgren, M., & Arnebrant, T. (1990). Adsorption of β-Lactoglobulin onto silica, methylated silica, and polysulfone. *Journal of Colloid and Interface Science*, *136*, 259–265.

Wang, Y., Chen, Z., Ba, T., Pu, J., Chen, T., Song, Y., Gu, Y., Qian, Q., Xu, Y., Xiang, K., Wang, H., & Jia, G. (2013). Susceptibility of young and adult rats to the oral toxicity of titanium dioxide nanoparticles. *Small (Weinheim an der Bergstrasse, Germany)*, *9*, 1742–1752.

Weir, A., Westerhoff, P., Fabricius, L., Hristovski, K., & Goetz, N. von (2012). Titanium dioxide nanoparticles in food and personal care products. *Environmental science & technology*, *46*, 2242–2250.

Wu, J., Liu, W., Xue, C., Zhou, S., Lan, F., Bi, L., Xu, H., Yang, X., & Zeng, F.-D. (2009). Toxicity and penetration of TiO2 nanoparticles in hairless mice and porcine skin after subchronic dermal exposure. *Toxicology letters*, *191*, 1–8.

Yusoff, R., Kathawala, M. H., Nguyen, L. T.H., Setyawati, M. I., Chiew, P., Wu, Y., Ch'ng, A. L., Wang, Z. M., & Ng, K. W. (2018). Biomolecular interaction and kinematics differences between P25 and E171 TiO2 nanoparticles. *NanoImpact*, *12*, 51–57.

Zhang, Y., Xu, B., Yao, M., Dong, T., Mao, Z., Hang, B., Han, X., Lin, Z., Bian, Q., Li, M., & Xia, Y. (2018). Titanium dioxide nanoparticles induce proteostasis disruption and autophagy in human trophoblast cells. *Chemico-biological interactions*, *296*, 124–133.